Sensitivity of nocturnal boundary layer temperature to tropospheric aerosol surface radiative forcing under clear-sky conditions

Udaysankar S. Nair,[1] Richard McNider,[2] Falguni Patadia,[1,3] Sundar A. Christopher,[1,2] and Kirk Fuller[1]

Received 17 February 2010; revised 6 October 2010; accepted 13 October 2010; published 22 January 2011.

[1] Since the middle of the last century, global surface air temperature exhibits an increasing trend, with nocturnal temperatures increasing at a much higher rate. Proposed causative mechanisms include the radiative impact of atmospheric aerosols on the nocturnal boundary layer (NBL) where the temperature response is amplified due to shallow depth and its sensitivity to potential destabilization. A 1-D version of the Regional Atmospheric Modeling System is used to examine the sensitivity of the nocturnal boundary layer temperature to the surface longwave radiative forcing (SLWRF) from urban aerosol loading and doubled atmospheric carbon dioxide concentrations. The analysis is conducted for typical midlatitude nocturnal boundary layer case days from the CASES-99 field experiment and is further extended to urban sites in Pune and New Delhi, India. For the cases studied, locally, the nocturnal SLWRF from urban atmospheric aerosols (2.7–47 W m^{-2}) is comparable or exceeds that caused by doubled atmospheric carbon dioxide (3 W m^{-2}), with the surface temperature response ranging from a compensation for daytime cooling to an increase in the nocturnal minimum temperature. The sensitivity of the NBL to radiative forcing is approximately 4 times higher compared to the daytime boundary layer. Nighttime warming or cooling may occur depending on the nature of diurnal variations in aerosol optical depth. Soil moisture also modulates the magnitude of SLWRF, decreasing from 3 to 1 W m^{-2} when soil saturation increases from 37% to 70%. These results show the importance of aerosols on the radiative balance of the climate system.

Citation: Nair, U. S., R. McNider, F. Patadia, S. A. Christopher, and K. Fuller (2011), Sensitivity of nocturnal boundary layer temperature to tropospheric aerosol surface radiative forcing under clear-sky conditions, *J. Geophys. Res.*, *116*, D02205, doi:10.1029/2010JD014068.

1. Introduction

[2] Surface air temperature observations in the last century show a clear trend of nighttime minimum temperatures increasing at a rate twice that of the daytime maximum temperature except during the 1979–2004 time period when the rate of increase of both maximum and minimum temperatures are approximately the same [*Dai et al.*, 1999; *Karl et al.*, 1984, 1993]. This asymmetry in the trends of maximum and minimum temperatures have decreased the diurnal temperature range (DTR) over the land surface throughout the globe with the exception of weak increases in central Canada and southeastern Australia [*Karl et al.*, 1993]. While the DTR decrease is present in every season, in the U.S. the largest decreases occur during the fall season with the smallest change in the spring [*Karl et al.*, 1993]. A more recent analysis [*Vose et al.*, 2005] does not show a strong seasonal difference for the Northern Hemisphere and in fact the largest decrease in winter. The 1979–2004 seasonal analysis shows the largest decrease in fall and smallest in spring although note that the number of stations from 1979 to 2004 are far less than in the 1950–1979 data set. There is considerable debate regarding the mechanisms responsible for the DTR decrease [*Intergovernmental Panel on Climate Change* (*IPCC*), 2007; *Dai et al.*, 1999]. Some suggested factors responsible for the increase in nocturnal minimum temperature include urban heat islands, greenhouse gases, clouds, land use changes, and tropospheric aerosols [*Balling and Cerveny*, 2003; *Braganza et al.*, 2004a; *Kalnay and Cai*, 2003; *Pielke et al.*, 2007; *Zhou et al.*, 2007]. Heat island effects would initially appear to be a viable mechanism because minimum temperatures are more susceptible to urban thermal inertia. While DTR climate trend analyses often attempt to remove these urban effects [*Karl et al.*,

[1]Earth System Science Center, University of Alabama in Huntsville, Huntsville, Alabama, USA.
[2]Department of Atmospheric Science, University of Alabama in Huntsville, Huntsville, Alabama, USA.
[3]Goddard Earth Sciences and Technology Center, University of Maryland, Baltimore County, Baltimore, Maryland, USA.

0148-0227/11/2010JD014068

1984], the effectiveness of such techniques are not well understood.

[3] General Circulation Model (GCM) sensitivity studies show that increased concentration of greenhouse gases such as CO_2 and CH_4 also cause changes in DTR. However, comparative studies with state-of-the-art GCMs reveal differences in the magnitude and even the sign of DTR trends among the models. These studies also reveal large discrepancies between modeled and observed DTR trends [*Cao et al.*, 1992; *Stone and Weaver*, 2003]. On the basis of these results, *Karl et al.* [1993] and *Stone and Weaver* [2003] concluded that the land surface parameterizations or physics in existing GCMs may not be robust enough to correctly capture the observed DTR signal. *Walters et al.* [2007] also proposed that the coarse resolution in GCMs may not correctly capture the sensitivity of the nocturnal boundary layer to either external forcing or parameters describing the land surface characteristics.

[4] Cloudiness trend is another factor that needs to be considered in interpreting observed DTR trends. *Dai et al.* [1999] examined the physical and statistical relationships of clouds, precipitation, and soil moisture in the First International Satellite Land Surface Climatology Project (ISLCP) Field Experiment (FIFE) data. They showed that clouds could change the DTR and that soil moisture was less important than clouds. Using this evidence and some historical measures of cloudiness trends, they concluded that cloudiness was the most likely cause of the DTR change. *Hansen et al.* [1995] showed that clouds were apparently the only adjustable GCM parameter that could damp the DTR to its observed magnitude. However, the GCMs often lack adequate vertical resolution in the nocturnal boundary layer (NBL) and do not include explicit treatment of aerosol microphysics. As will be shown in this paper, aerosols would provide a similar response signal to that of a change in cloudiness. Further, while cloudiness trends are uncertain, anthropogenic aerosol loading in the atmosphere has definitively increased in the last century [*Ramanathan et al.*, 2001a]. Recently, *Kalnay and Cai* [2003] conducted a long-term reanalysis of modeled and observed data. Their study showed that changes in land surface usage, including irrigation, contribute significantly to the observed DTR trends. Irrigation would have the expected effect of lowering daytime temperatures due to evaporation and raising nighttime temperatures due to the higher heat capacity of wet soils and well-hydrated vegetation. However, rigorous statistical verification of this mechanism would be difficult because surface moisture availability is not routinely measured. Moreover, the DTR has decreased in some areas where irrigation effects would be minimal, such as the eastern United States. All in all, with the uncertainties in long-term cloudiness trends and the persistent deficiencies in GCM surface land processes, there is still considerable uncertainty in explaining the DTR trends.

[5] Increases in tropospheric aerosol concentrations have also been suggested as a significant factor in the DTR trends [*Stone and Weaver*, 2003; *Braganza et al.*, 2004a, 2004b; *Makowski et al.*, 2008]. *Makowski et al.* [2008] attributes long-term trends in DTR mostly to modulation of incoming solar radiation through the direct and indirect aerosol effect. Most aerosol studies [*IPCC*, 2007] have concentrated on the direct radiative effect of aerosol scattering and the indirect effects of aerosols in clouds (see *Yu et al.* [2002] for a comprehensive review). Both effects tend to increase the planetary albedo and reduce daytime temperatures. Recent global scale aerosol studies [*Koch et al.*, 2007] have begun to demonstrate the importance of carbonaceous aerosols, especially elemental carbon (EC), to the atmospheric aerosol budget. EC aerosols serve as net warmers of the planetary boundary layer (PBL) and the free troposphere. This effect would counter aerosol cooling in the daytime and reduce surface cooling at night. Detailed reviews of aerosol measurement and modeling studies [*IPCC*, 2007] have concluded that the foregoing aerosol effects are potentially significant (with magnitudes comparable to the predicted warming from greenhouse gases) but also very poorly understood (the magnitude of the net uncertainty is comparable to the aerosol effects; the sign is unknown).

[6] The majority of research studies on aerosol radiative interactions focus on the daytime interaction of aerosols with solar radiation through both direct and indirect pathways. However, there are relatively few studies that address the radiative impact of aerosols on the nocturnal boundary layer [*Estournel et al.*, 1983; *Garratt et al.*, 1990; *Jacobson*, 1997; *Venkatram and Viskanta*, 1977; *Yu et al.*, 2002; *Zdunkowski et al.*, 1976]. Even though these studies address various aspects of aerosol radiative interaction with NBL, a systematic analysis that includes spatiotemporal variations of the NBL and aerosols is lacking. *Zdunkowski et al.* [1976] conducted a detailed analysis of the impact of air pollution on PBL including the hygroscopic growth of aerosols. While the numerical modeling experiments of *Zdunkowski et al.* [1976] did not explicitly consider effects of diurnal asymmetries in atmospheric aerosol loading (diurnal variations in aerosol optical depth (AOD) resulting from changes in aerosol mass concentration, chemical composition, particle size, etc.), they noted that dense haze cover at nighttime following a clear day will lead to warming at the surface. *Jacobson* [1997] used a detailed air pollution modeling system to examine the impact of aerosols on the PBL, including nocturnal effects. Even though the modeling system captured the diurnal variability of aerosol loading, the study did not focus on the role of nocturnal heating and DTR trends.

[7] The purpose of this study is to investigate the response of the nocturnal boundary layer to longwave aerosol radiative forcing. Simple models [*Pielke and Matsui*, 2005] have indicated that due to the shallow nature of the nocturnal boundary layer under light winds, the temperature response to longwave forcing may be large. Additionally, *Walters et al.* [2007] showed that the forcing itself may change the boundary layer height causing a mixing of heat down from aloft. This mixing of heat from aloft has a multiplying effect on the direct warming of the boundary layer due to the added radiation. While both of these studies dealt with increases in downward longwave radiation into the surface from greenhouse gases, similar responses might be expected from downward longwave radiation to the surface from aerosols. Also, both of these studies employed simple models. *Pielke and Matsui* [2005] employed a semiempirical analytical formulation that did not incorporate full nonlinear dynamics between the surface and the atmosphere. *Walters et al.* [2007], while including full nonlinear interaction with the surface, employed only a two-layer atmosphere. The

Table 1. Description of the Numerical Experiments Utilized in This Study

Experiment Name	Description
C1	1-D simulation initialized using CASES-99 radiosonde observation acquired at 0 UTC on 21 Oct 1999. Clear atmosphere and carbon dioxide concentration of 370 ppm (average value for 1999) are used.
U1	Same as C1 except for the assumption of urban aerosol loading.
U2	Same as U1 except for the assumption of zero nighttime AOD.
U3	Same as U1 except for the reduction of daytime AOD by a factor of 2.
X2	Same as C1 except for the assumption of doubling atmospheric CO_2 concentration from present-day values to 760 ppm.
D1	Same as C1 except for the assumption of desert dust aerosol loading.
C2	Same as C1 except for the assumption of constant soil saturation of 70%.
U4	Same as U1 except for the assumption of constant soil saturation of 70%.
U5	Urban land surface characteristics and aerosol optical characteristics deduced for Pune [*Panicker et al.*, 2008].
C3	Same as U5 except for the assumption of an aerosol-free atmosphere.
U6	Urban land surface characteristics, aerosol optical characteristics deduced for New Delhi [*Singh et al.*, 2005].
C4	Same as U6 expect for the assumption of an aerosol-free atmosphere.

present study will examine the response of a full nonlinear multilevel atmospheric model (a 1-D version of the Regional Atmospheric Modeling System (RAMS)) to aerosol radiative forcing. The experimental design and description of the numerical modeling system used are described in section 2, while results, discussion of the analysis, and conclusions are presented in sections 3, 4, and 5, respectively.

2. Methodology

2.1. Experimental Design

[8] The primary goal of this study is to assess the immediate direct effect of surface longwave radiative forcing (SLWRF) from urban aerosols on the nighttime surface air temperatures and gain an understanding of conditions and processes through which surface air temperature is impacted. A comparison of the impact of SLWRF from atmospheric aerosols to doubled atmospheric carbon dioxide is also of interest. This is achieved by conducting a sensitivity analysis of typical cases of observed, stable nocturnal boundary layer (SNBL) development using a 1-D version of RAMS. While this study is a sensitivity analysis, it is important to note that the experiments are based on a nocturnal boundary layer that has the physical attributes of observations. As noted by *Steeneveld et al.* [2006] and *Walters et al.* [2007], models often have difficulties capturing the dynamic range of boundary layer cooling at night due to anomalous numerical diffusion or profile formulations that preclude strong stability. Such models will not be sensitive in resolving the effects of relatively small perturbations in longwave radiation at the surface. Thus, this study adopts an experimental design where RAMS is used to simulate typical SNBL case study days of 21–22 October 1999 from the Cooperative Atmosphere-Surface Exchange Study [*Poulos et al.*, 2002] held in 1999 (CASES-99) near Leon, Kansas (37.65°N, 96.73°W) with the objective of improving the understanding of processes relevant to the SNBL. The days used in this study are typical SNBL case days that were the focus of other modeling studies [*Steeneveld et al.*, 2006]. The experimental design utilized in this study establishes the capability of the model to faithfully simulate these typical SNBL case days by comparing model simulations against detailed field observations of surface meteorology and energy fluxes collected during CASES-99.

[9] Sensitivity experiments are then conducted for these case days by modifying the validated control experiment (C1), by including radiative forcing from typical urban aerosols (U1) and doubled atmospheric carbon dioxide (X2, see Table 1 for description of all the experiments). Additional sensitivity experiments, U2 and U3 are conducted to examine the impact of diurnal variation in atmospheric aerosol loading, D1 to address the impact of other aerosol types on SNBL development, while C2 and U4 are used to examine how soil moisture modulates the impact of aerosol surface radiative forcing on surface air temperature.

[10] The analysis is then extended to urban locations where detailed observations are not available for initialization and validation, but for which aerosol characterization is available. The experiments U5 and U6 utilize urban aerosol composition characteristic of two urban sites in India, namely Pune [*Panicker et al.*, 2008] and New Delhi [*Singh et al.*, 2005], respectively, valid for the time period December 2004 to January 2005 and April to June 2003, respectively. The U5 and U6 experiments are compared against C3 and C4, which are experiments that are identical to U5 and U6, except for the assumption of clear air conditions in order to examine whether the results obtained for CASES-99 site is also applicable to other areas.

[11] Note that the experiments used in this study are not climate experiments since they do not look at the cumulative impact of either aerosols or greenhouse gases. Rather, they provide an examination of the direct sensitivity of NBL to these forcings.

2.2. Description of RAMS

[12] This study utilizes RAMS, Version 4.4, modified to include radiative interactions of aerosols, to study the impact of aerosols on nocturnal boundary layer development. RAMS is a nonhydrostatic atmospheric model used to simulate a wide range of atmospheric phenomenon [*Cotton et al.*, 2003] and utilizes finite difference approximations to solve conservation equations of mass, momentum, heat, and different water phases. Cloud and precipitation processes are represented in the model through either convective parameterization or explicit parameterization of cloud microphysics. RAMS provides a variety of options with varying sophistication for representing subgrid scale turbulence. Land surface processes are simulated using a multilayer soil model and the Land Ecosystem Atmosphere Feedback (LEAF-2) model [*Walko et al.*, 2000]. While radiative transfer schemes of varying complexity [*Mahrer and Pielke*, 1977; *Chen and Cotton*, 1983; *Harrington et al.*, 1999] are available in RAMS, none account for radiative interactions with aerosols. RAMS was modified to include a Delta four-

Table 2. Composition of Aerosol Models Used in the Study[a]

Aerosol Model	Composition			0.55 μm AOD (80% Relative Humidity)
	Component	Number Density (cm^{-3})	Mode Radius (μm)	
Urban (U1)	Water soluble	28,000	0.0212	0.643
	Insoluble	1.5	0.471	
	Soot	130,000	0.0118	
Urban (U4) [*Panicker et al.*, 2008]	Water soluble		0.0212	0.347
	Insoluble		0.471	
	Soot		0.0118	
Urban (U5) [*Singh et al.*, 2005]	Soot	130,000	0.0118	0.863
	Water soluble	10,000	0.0212	
	Mineral, nucleation mode	269.5	0.07	
	Mineral, accumulation mode	5.050	0.39	
	Mineral, coarse mode	3.850	1.90	
Desert (D1)	Water soluble	0.018	0.0212	0.286
	Mineral, nucleation mode	0.033	0.07	
	Mineral, accumulation mode	0.747	0.39	
	Mineral, coarse mode	0.202	1.90	

[a]Log-normal distribution is assumed for aerosol model components whose subcomponents are as follows: water soluble: mixture of sulfates, nitrates and organics; insoluble: mixture of soil particles and organic material; soot: black carbon; mineral: mixture of quartz and clay [*Hess et al.*, 1998]. Note that the experiments in which these aerosol models are utilized are shown within parentheses next to the name of aerosol model in the first column.

stream radiative transfer scheme of *Fu and Liou* [1993], referred hereafter as FL-RTS [*Wang and Christopher*, 2006; *Wang et al.*, 2006]. Aerosol characterization within FL-RTS is based on the Optical Properties of Aerosols and Clouds (OPAC) based on *Hess et al.* [1998].

2.2.1. The FL-RTS

[13] The FL-RTS is a plane-parallel radiative transfer model [*Fu and Liou*, 1993] that computes upwelling and downwelling radiative fluxes at specified, discrete locations within an atmospheric column. The FL-RTS divides the radiation spectrum into six broadbands in the shortwave (SW) part (0.2–4 μm), with the first band (0.2–0.7 μm) being subdivided into 10 subbands. The longwave (LW) part of the spectrum (4–37.5 μm) is subdivided into twelve broadbands. Gaseous absorption characteristics within these bands are computed using the correlated k distribution method [*Fu and Liou*, 1992]. A delta function is used to model the forward scattering by clouds and aerosols. The FL-RTS provides the option to be configured either in the two or four stream mode for radiative flux computations. *Fu and Liou* [1993] show that the FL-RTS irradiance estimates are within 0.05% of line-by-line calculations.

2.2.2. The OPAC Aerosol Types

[14] The OPAC is a software package for specifying optical properties of clouds and aerosols as a function of wavelength. Single scattering albedo (ω_o), as well as asymmetry parameter (g) and extinction coefficients (β_{ext}) for individual aerosol components and aerosol types (mixture of components) are available at 61 wavelengths between 0.25 and 40 μm and at eight relative humidity values between 0%–99%. These optical properties along with vertical distribution information are needed to specify aerosol radiative interactions in the model. The OPAC assumes a lognormal size distribution for aerosols. Optical properties of individual components are computed assuming number concentrations of 1 cm^{-3} and therefore, need to be scaled appropriately for differing situations. Aerosol types in OPAC range from clean and polluted continental conditions to Arctic and Antarctic types that are composed of specific mixes of individual components. The OPAC aerosol types utilized in this study, namely urban and desert types differ both in composition and microphysics (Table 2). Urban aerosol types are a mixture of water soluble and soot components at a high number concentration but their particle size is smaller when compared to the desert aerosol types which are dominated by accumulation and coarse mode mineral components (see Table 2). This study specifically focuses on urban and dust aerosol types since prior studies report substantial SLWRF associated with these aerosol types and thus the potential to impact SNBL evolution. The other two aerosol types considered in this study are essentially OPAC aerosol types modified to conform to characteristics of urban aerosols observed over Pune and New Delhi, India, as reported by *Panicker et al.* [2008] and *Singh et al.* [2005]. The aerosol type for Pune, India, valid for the time period December 2003 through January 2004, is the OPAC Urban type with the number density of the components modified (Table 2) to match the observed AOD, single scattering albedo (SSA), and asymmetry parameter (ASP). Using a similar approach, *Singh et al.* [2005] found the premonsoon aerosol characteristics to be a mixture of the OPAC urban and desert aerosol types (Table 2).

2.2.3. Calculation of Aerosol Optical Thickness

[15] In FL-RTS, the aerosol optical depth (AOD) is computed following *Hess et al.* [1998] by assuming exponentially decreasing number concentrations with height as given by equation (1):

$$N(z) = N(0)e^{-\frac{z}{H}}, \tag{1}$$

where z is the altitude above ground in kilometers and H is the scale height in kilometers. The scale height specifies the nature of decrease of number concentration with height, with increasing values describing smaller variation with height. On the basis of the aerosol vertical distribution

Table 3. Numerical Model Configuration Used in the Different Experiments

Configuration	Experiments C1-C2, U1-U4, D1, X2	Experiments C3-C4, U5-U6
Vertical grid spacing at the surface	0.5 m	5 m
Grid stretch ratio	1.16	1.1
Maximum vertical grid spacing	500 m	500 m
Soil levels (below ground)	0.05, 0.075, 0.15, 0.225, 0.375, 0.60, 0.90 m.	0.001, 0.05, 0.1, 0.2, 0.3, 0.5, 0.7 m
Soil type	Clay loam [*Chen et al.*, 2007]	C3, U5: sandy soil C4, U6: silt loam [*Zobler*, 1999]
Land use	Short grass	Urban and built-up
Diffusion scheme	Vertical: Mellor-Yamada Horizontal:	Vertical: Mellor-Yamada Horizontal:
[*Cotton et al.*, 2003]	Modified Smagorinsky	Modified Smagorinsky
Initial atmospheric conditions	Radiosonde observations at 0 UTC (1800 LST)	Radiosonde observations at 1200 UTC (1730 LST)

described by (1), the AOD of an atmospheric layer contained between height levels z_1 and z_2 ($z_1 < z_2$) is given by

$$\tau_\lambda(z_1, z_2) = \int_{z_1}^{z_2} \beta_{\text{ext}}(z = 0, \lambda, \text{RH}) e^{-\frac{z}{H}} \mathrm{d}z = \beta_{\text{ext}}(z = 0, \lambda, \text{RH}) H \left(e^{-\frac{z_1}{H}} - e^{-\frac{z_2}{H}} \right), \quad (2)$$

where λ is the wavelength and RH is relative humidity. For each aerosol type, OPAC outputs β_{ext} at $z = 0$, which is computed using specified number concentrations of individual components. OPAC specifies the total physical thickness of urban and desert aerosol layers as 2 and 6 km and the scale heights to be 8 and 2 km, respectively. On the basis of these parameters, the computed values of AOD at 0.55 μm and 80% RH for urban and desert aerosol types are 0.643 and 0.286, respectively. The OPAC urban AOD is consistent with values over polluted regions in Africa, India, and China [*Ramanathan et al.*, 2001b; *Smirnov et al.*, 2002; *Pandithurai et al.*, 2007]. Since OPAC provides the optical properties only at eight discrete RH values, linear interpolation is used to determine aerosol optical properties at other RH values. Note, in addition to the mixed layer aerosol types, OPAC also suggests the use of a background aerosol type for the free troposphere ($\tau \sim 0.013$), stratospheric aerosol layer ($\tau \sim 0.005$), and if applicable, a transported mineral aerosol layer ($\tau \sim 0.097$). In this study, only the impact of the boundary layer aerosols is considered and the effect of other categories is ignored.

2.3. Numerical Model Configuration

[16] Numerical experiments in this study consist of 1-D simulations of atmospheric boundary layer development over a 48 h period, starting from initial conditions that are characterized by evening radiosonde observations. A pseudo 1-D configuration of RAMS is used to simulate atmospheric boundary layer development over a domain of 5 × 5 grid points with cyclic boundary conditions applied along the lateral boundaries. A sufficiently large grid spacing of 10 km in the x and y directions is utilized so that the model is incapable of resolving large eddies. Vertical grid structure, surface characteristics, and other relevant information are provided in Table 3.

[17] For the CASES-99 case days, when the soil model is directly initialized using soil moisture observations, model-simulated latent heat fluxes are negligible compared to observations. Latent heat flux observations are not negligible however and thus suggest that while the local soil moisture observations in the 0–25 cm layer are dry, it may not be reflective of large-scale conditions. Therefore, the soil moisture content in this layer was systematically altered until close agreement was obtained between observations and model-simulated sensible and latent heat fluxes, 2 m temperature, and relative humidity. The altered soil moisture profile was utilized in all the other experiments.

[18] In the urban site experiments (U5–U6), soil moisture and temperature observations are not available and therefore information from the National Center for Environmental Prediction (NCEP) Reanalysis data set was utilized to initialize the soil model. Note that the soil moisture values from the NCEP Reanalysis are average conditions for 2.5° × 2.5° grid cell. Similar to the C1 experiment, the soil moisture was adjusted until there is relatively good agreement between the 2 m temperature, relative humidity simulated by the U5 and U6 experiments and the corresponding observations.

3. Results

[19] The sensitivity analyses discussed in the following sections utilize specific days from CASES-99 (21–22 October 1999). Additional experiments conducted for the time period 23–25 October 1999 (CASES-99 days) yielded similar results and thus are excluded for brevity.

3.1. Comparison of the CASES-99 Control Simulation (C1) to Observations

[20] Observations of downwelling solar radiation (Figure 1a) show the presence of clouds in the time period centered around local solar noon on both 21 and 22 October 1999 making comparisons to model simulations complicated. Cloud cover appears to be more optically thick and persistent on 21 October when compared to 22 October. A comparison with observations from 22 October shows the model simulation generally overestimating the downwelling shortwave with a maximum difference of 61 W m^{-2}. During the late afternoon hours on both days, when clouds are not present, mean error between model simulation and observations is approximately 5%, slightly higher than the 3% error estimated by *Christopher et al.* [2003].

[21] Model-simulated downwelling longwave radiation at the surface (Figure 1b) compares well with observations during both nights (with a difference of less than 2%), while there are considerable differences during the first day (maximum of 18%). Substantial daytime differences during the first day may be related to the presence of clouds. On the second day, there is better agreement between the simulation

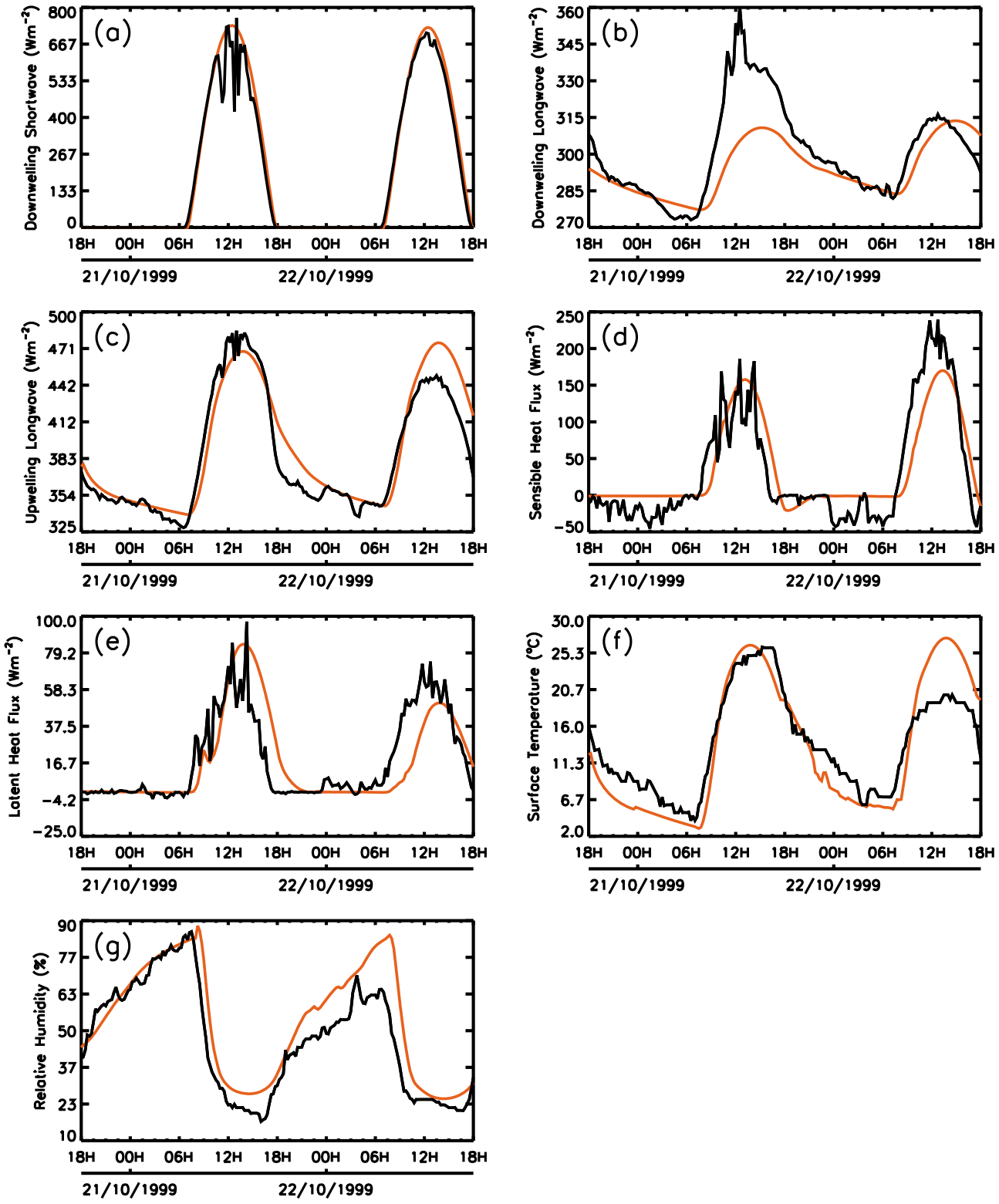

Figure 1. Comparison between observations (black line) and C1 simulation (red line) of (a) downwelling shortwave, (b) downwelling longwave, (c) upwelling longwave, (d) sensible heat flux, (e) latent heat flux, (f) surface air temperature, and (g) relative humidity.

and observations during the morning hours, but larger deviations occur in the afternoon. However, note that there was a frontal passage through the area at this time, which the pseudo 1-D model does not capture. During the second night, the model and the observations resume a close agreement, with the differences averaging to less than 2%.

[22] There is good agreement between the observed and model-simulated upwelling longwave radiation from the

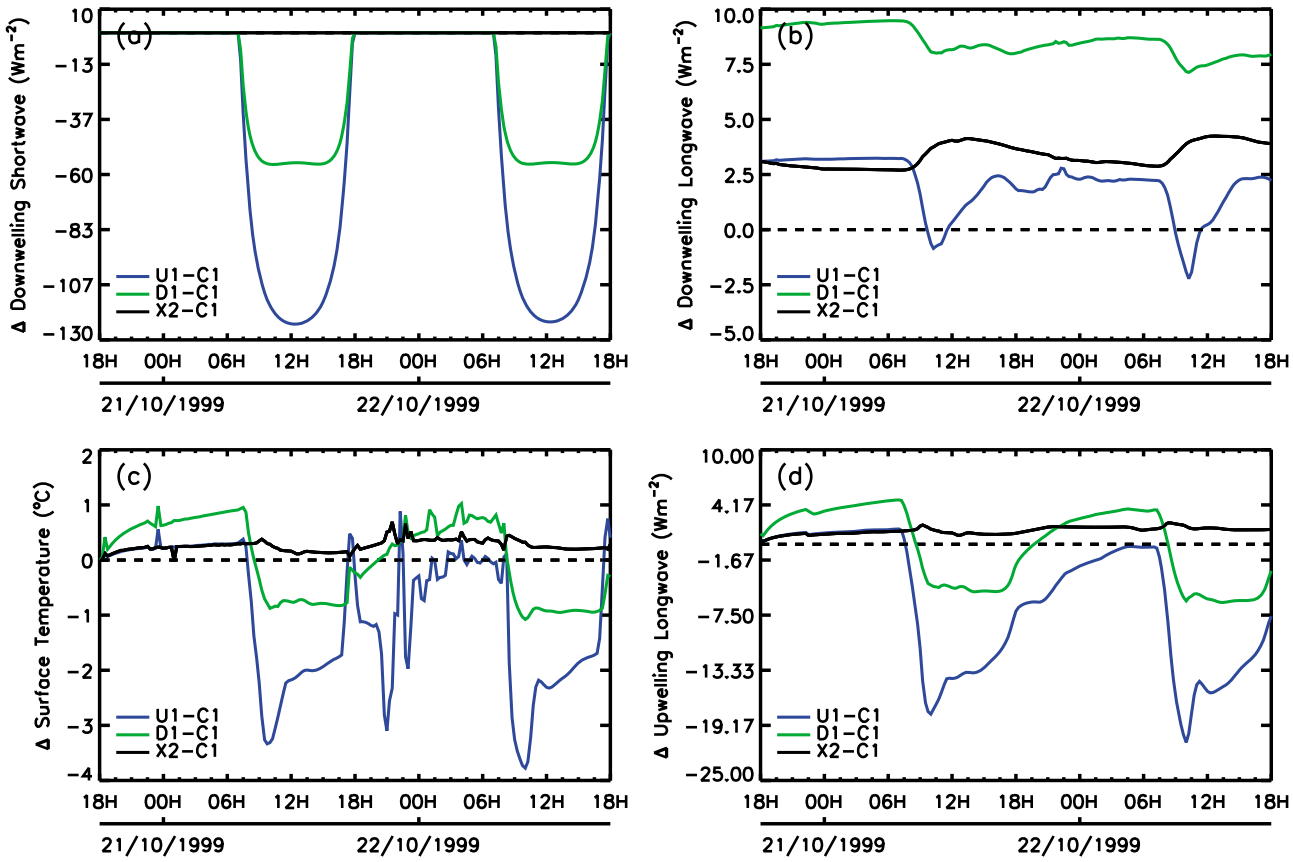

Figure 2. Differences in (a) downwelling shortwave fluxes, (b) downwelling longwave fluxes, (c) surface air temperature, and (d) upwelling longwave fluxes between the U1 and C1 (blue), D1 and C1 (green), and X2 and C1 (black solid) experiments. Zero difference value is shown in Figures 2a–2d using the black dashed line.

surface (Figure 1c), except during the afternoon hours of the second day when the frontal passage occurred. Simulated patterns of surface sensible and latent heat fluxes (Figures 1d and 1e), though very similar to observations, lag the observations by approximately half an hour. The heat and moisture fluxes show substantial variability during the first day due to cloudiness. During the second day, the variability is much less and the maximum amplitudes of observed and simulated patterns of sensible and latent heat fluxes differ by ~40 and 15 W m^{-2}, respectively. The RAMS simulations of temperature (Figure 1f) and humidity (Figure 1g) patterns are also consistent with observations during the first day but differ during the second day due to frontal passage, when the observed surface temperature and relative humidity are substantially lower in comparison to model-simulated values.

3.2. Radiative Impact of Urban Aerosols and Doubled Carbon Dioxide

[23] While the top-of-atmosphere shortwave and longwave radiative forcing metrics are utilized in Earth radiation budget studies, radiative forcing at the surface is the metric that is most relevant for this study. For given land surface conditions, the surface air temperature, heat, and moisture fluxes to the atmosphere are most sensitive to the net radiative energy available at the surface. Thus surface shortwave and longwave radiative forcing are the appropriate metrics for analyzing the impact of atmospheric aerosols on boundary layer development and will be utilized in the analysis of the experiments conducted in this study.

[24] In the shortwave part of the spectrum, when comparing the control (C1), urban aerosol (U1) and doubled CO_2 experiments (X2), substantial differences are observed only between the C1 and U1 experiments (Figure 2a). The downwelling shortwave radiation at the surface is substantially reduced in the U1 experiment, with differences of up to 123 W m^{-2} occurring at the local solar noon hour. Since carbon dioxide is not a major absorber in the shortwave, there is very little difference in the downwelling shortwave flux at the surface between the X2 and C1 experiment.

[25] However, in the longwave, there are substantial differences between the U1, X2, and the C1 experiment (Figure 2b). During the first night, both U1 and X2 show enhancement in downwelling longwave of approximately 3.0 W m^{-2} compared to the C1 experiment. During the second night, the enhancement in downwelling longwave in the U1 simulation reduces to ~2.2 W m^{-2}. This reduction during the second night is related to reduced water vapor loading in the U1 simulation due to attenuation of downwelling shortwave radiation leading to less evaporation and transpiration. The nocturnal enhancement in downwelling longwave radiation is within the range (2.5–16 W m^{-2}) reported by prior studies [*Estournel et al.*, 1983; *Jacobson*,

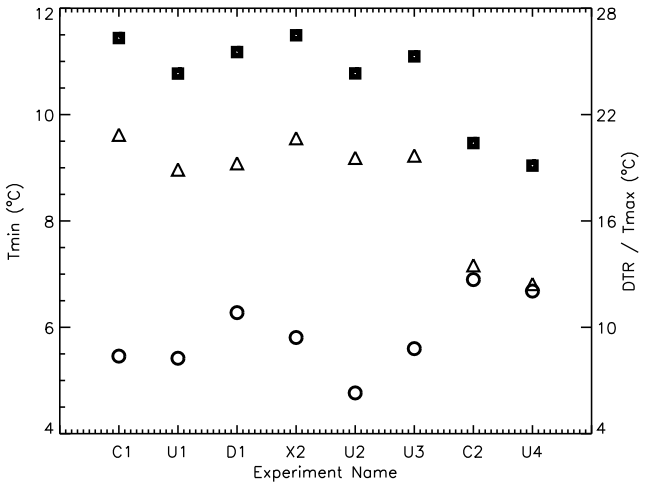

Figure 3. Diurnal temperature range (open triangle), maximum (solid square), and minimum (open circle) temperatures for the different experiments. The values are valid for the time period including the first day and the second night.

1997; *Panicker et al.*, 2008; *Zdunkowski et al.*, 1976], closer to lower limits. The nighttime differences in downwelling longwave between U1 and X2 are minimal during the first night (~0.1–0.2 W m^{-2}) and are more substantial during the second night (~1 W m^{-2}). During the daytime, the differences in downwelling longwave between the C1 and U1 simulations are substantially greater with a maximum value of approximately 4.5 W m^{-2} reflecting differing vertical distributions of aerosols and carbon dioxide. Note that the urban aerosols are confined to the lowest 2 km while carbon dioxide is assumed to be well mixed through the depth of the model atmosphere. Thus, under clear-sky conditions, carbon dioxide is able to better absorb and reradiate enhanced longwave emissions from the surface and the PBL during the daytime.

3.3. Impact of Urban Aerosols and Doubled Carbon Dioxide on Surface Air Temperature

[26] In the CASES-99 experiments, enhancement in nocturnal downwelling longwave radiation due to urban aerosol loading and doubling of carbon dioxide leads to an increase in surface air temperature during the first night (Figure 2c). The nocturnal minimum is increased by ~0.38°C and 0.3°C during the first night in U1 and X2 experiments, respectively. During the first day of the simulation, substantial reduction of downwelling shortwave radiation at the surface is accompanied by reduction in daytime surface air temperature in the U1 experiment with a maximum difference of ~2°C occurring in the afternoon (Figure 3). The surface air temperature in the X2 simulation shows a very small increase when compared to the C1 simulation, with a maximum difference of less than 0.16°C (Figure 3) occurring in the afternoon. Note that the small increase in daytime surface air temperature in the X2 experiment is primarily due to enhancement in downwelling longwave radiation at the surface.

[27] The impact of doubled carbon dioxide on surface air temperature during the second night is very similar to that found during the first night. The solutions of surface air temperature are similar in both the C1 and X2 simulations but start diverging later in the night with the surface air cooling at a faster rate in the C1 simulation. Nocturnal minimum temperature in the C1 simulation is smaller than that found in the X2 simulation by ~0.35°C. The net effect of doubled carbon dioxide on the surface air temperature cycle is reduction of DTR (Figure 3). Enhancement in DTR due to a small increase in daytime maximum temperature is offset by a substantially larger increase in nocturnal minimum temperature, causing the net effect of doubled atmospheric carbon dioxide to be a reduction in DTR.

[28] However, the behavior of the U1 simulation is considerably different on the second night. The surface air temperature in the U1 simulation is initially cooler compared to the C1 simulation, but the solutions converge to similar values at early morning hours (Figure 2d). These patterns (Figures 2c and 2d) suggest that daytime cooling of the surface during the first day, leads to cooler surface air temperature going into the second night. But, by the end of the second night, enhancement in downwelling longwave radiation at the surface in the U1 simulation causes the nocturnal minimum temperature to be approximately the same as that in the C1 simulation. This is verified by the U2 simulation, where the aerosol optical depth is set to zero at nighttime, which shows that without the longwave enhancement (Figure 4a), surface air temperature remains cooler compared to the C1 simulation (Figure 4b), yielding lower nocturnal minimum temperatures (Figure 3) and an increase in DTR of ~0.66°C (Figure 3). RAMS simulation experiments show that the impact of urban aerosols is to reduce the DTR by reducing the daytime maximum and increasing the nocturnal minimum temperature.

4. Discussion

[29] RAMS simulations show that heavy aerosol loading and characteristics of conditions in polluted regions around the globe such as India and China have a substantial impact on surface air temperature and the radiation budget. Nocturnal SLWRF due to heavy urban aerosol loading and direct radiative effects of doubled atmospheric carbon dioxide at local scales are comparable for the cases considered in this study (see section 3.2). Therefore, on a local scale, urban aerosols have the potential to impact nocturnal boundary layer temperature. Since many of the temperature observations around the globe used in the DTR trend analysis are made in urban settings, the local effects may have a significant impact on such trends.

[30] This study illustrates that the response of the SNBL surface air temperature to perturbations in the surface radiation budget is disproportionate when compared to the convective boundary layer (CBL). Nocturnal boundary layer processes and their sensitivity to changes in both radiation input and surface properties are relevant to interpreting trends in surface air temperature and DTR. Note that a nocturnally averaged radiative forcing of 3.2 W m^{-2} resulted in an average surface air temperature increase of 0.22°C during the first night in the U1 experiment, while a daytime average radiative forcing of −84 W m^{-2} leads to an average daytime surface air temperature cooling of 1.5°C. The sensitivity of surface air temperature to perturbations in down-

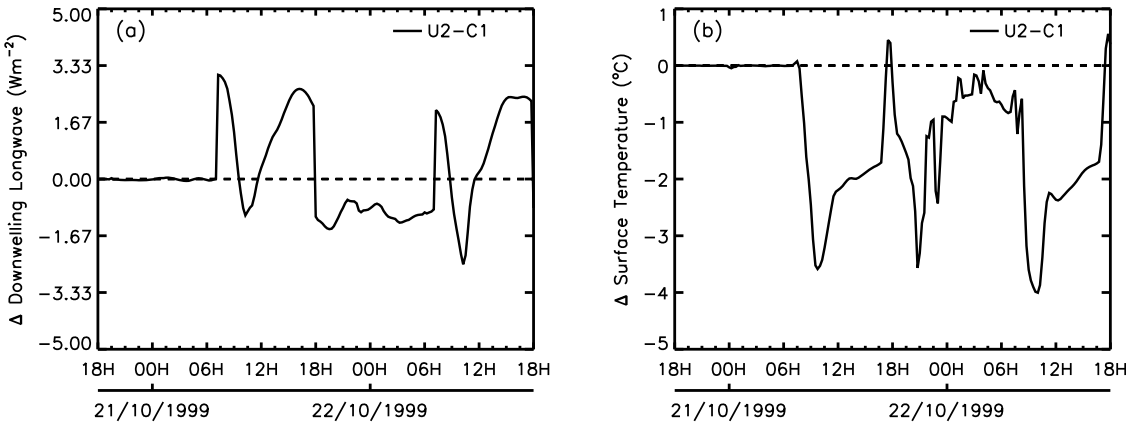

Figure 4. Differences in (a) downwelling longwave fluxes at the surface and (b) surface air temperatures between the U2 and C1 experiments. Zero difference value is indicated in Figures 4a and 4b using the dashed line.

welling radiation (δ) due to urban aerosol loading may be quantified as

$$\delta = \frac{\Delta \overline{T}_a}{\Delta \overline{F}_\downarrow} \tag{3}$$

where $\Delta \overline{T}_a$ and $\Delta \overline{F}_\downarrow$ are average differences in surface air temperature and average forcing of downwelling radiation at the surface due to urban aerosol loading. The δ values computed separately for NBL (δ_{NBL}) and CBL (δ_{CBL}) occurring during the first 24 h of the U1 simulation yields values of 0.068 and 0.018 K/W m^{-2}, respectively. Thus, the sensitivity of the SNBL surface air temperature to SLWRF radiative forcing from urban aerosol loading is 3.7 times more than that of the CBL. This difference in sensitivity is largely due to the differences in depth of the CBL and NBL. *Walters et al.* [2007] examined temperature sensitivity of NBL to arbitrarily prescribed SLWRF using a two-layer atmosphere and found a sensitivity of about 0.12 K/W m^{-2} in the light wind and very stable NBL and about 0.04 K/W m^{-2} in the weakly stable NBL (see discussion and Figure 7 below). Thus, the results of this more complete boundary layer model are in keeping with the simple model employed by *Walters et al.* [2007]. The magnitude of SLWRF is reduced during nighttime due to the smaller radiating temperature of the lower part of the atmosphere. However, the smaller depth of the NBL confines this heating to a smaller depth [*Walters et al.*, 2007] leading to a larger temperature response and thus sensitivity.

[31] In the specific cases considered in this study, the magnitude of daytime reduction in surface air temperature dominates over the nocturnal warming leading to an overall cooling effect. However, the overall effect could be different depending on several factors, including aerosol optical characteristics, diurnal variations in column loading and vertical distribution of aerosols, and nocturnal boundary layer dynamics. For example, in the model simulations of *Jacobson* [1997] over the Los Angeles Basin, urban aerosols with differing optical characteristics caused a daytime cooling of 0.08 K, a maximum reduction in shortwave of 55 W m^{-2} (150 W m^{-2} in the present study), nocturnal warming of 0.77 K, and maximum nocturnal longwave enhancement of 13 W m^{-2} (4.0 W m^{-2} in the present study). Other studies also report larger magnitudes for nocturnal enhancement of longwave in the presence of urban aerosols [*Estournel et al.*, 1983; *Panicker et al.*, 2008; *Welch and Zdunkowski*, 1976]. The study also examined the impact of other OPAC aerosol models on boundary development

Table 4. Differences in Downwelling Shortwave, Upwelling Longwave, Sensible, and Latent Heat Fluxes Between the Different Experiments[a]

	Downwelling Shortwave (W m^{-2})			Upwelling Longwave (W m^{-2})			Sensible Heat (W m^{-2})			Latent Heat (W m^{-2})		
Δ	T_{min1}	T_{max1}	T_{min2}	T_{min1}	T_{max1}	T_{min2}	T_{min1}	T_{max1}	T_{min2}	T_{min1}	T_{max1}	T_{min2}
U1-C1	−34.13	−121.25	−9.65	−9.59	−13.58	−0.41	−0.19	−30.55	−0.01	−0.10	0.01	−0.01
D1-C1	−22.23	−55.35	−5.85	−6.10	−4.93	3.63	−0.07	−0.10	−0.05	−0.02	3.94	0.03
X2-C1	0.00	−0.01	−0.00	1.41	1.21	1.64	−0.00	7.49	−0.01	0.01	3.80	0.01
U2-C1	−34.13	−121.27	−21.26	−0.69	−13.56	−2.06	−0.19	−34.92	0.25	−0.10	−7.13	−0.21
U3-C1	−23.79	−64.08	−7.64	0.71	−7.08	0.50	−0.14	−24.92	−0.00	−0.08	−7.18	−0.03
U4-C2	−34.12	−139.76	−20.99	0.55	−7.73	−0.52	−0.15	−24.49	0.09	−0.19	−56.97	−0.01
U5-C3	−13.79	−26.21	−13.59	2.12	−6.41	0.27	−0.84	−46.71	0.09	0.30	−24.99	0.03
U6-C4	10.78	−254.33	23.20	5.45	−9.48	10.34	−2.06	−121.36	−0.94	24.56	−32.84	17.68

[a]The experiments for which the differences are computed are given in column 1. Differences are computed for the times corresponding to the occurrence of minimum and maximum surface temperatures during the first night-day cycle (T_{min1}, T_{max1}) and the minimum temperature for the following night (T_{min2}).

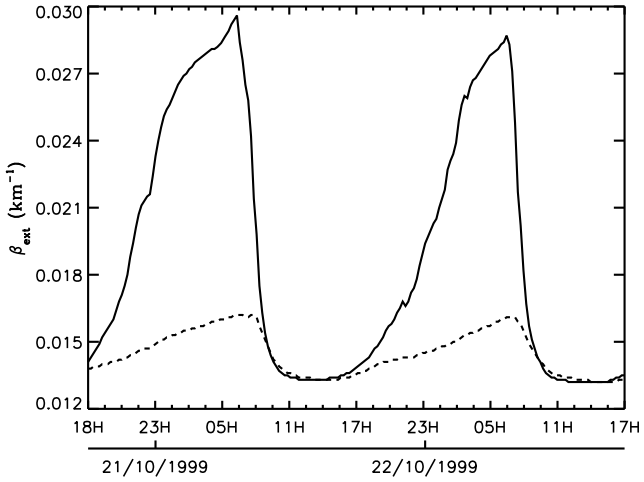

Figure 5. Diurnal variation of aerosol extinction coefficient in the infrared (10.2–12.5 μm) in the U1 experiment at the first model level (solid line) and averaged for the atmospheric column in the lowest 100 m (dashed line).

and found desert aerosols to be the only type capable of producing longwave forcing similar to *Jacobson* [1997]. The D1 simulation, where the OPAC desert aerosol optical model is used, shows a nocturnal downwelling longwave radiation increase of 9 W m^{-2} (Figure 2b) leading to nocturnal surface air temperature increases of more than 1 K (Figure 2c) and a depression in DTR of ~1.6°C (Figure 3).

[32] Differences in nocturnal surface air temperature evolution between the first and second nights in the U1 simulation (Figure 2c and Table 4), resulting from differing amounts of daytime surface heating, suggest that diurnal variations in aerosol column loading and vertical distribution are important factors in determining the overall impact on DTR and average surface air temperature. Constant aerosol composition and number concentrations are assumed in the aerosol experiments used in this study and the temporal variations in aerosol optical depth is solely due to the hygroscopic effect (Figure 5). However, in reality, time-varying emissions and atmospheric circulation patterns lead to diurnal asymmetries in aerosol composition, number concentrations, and vertical distribution [*Allen et al.*, 1999; *Dorsey et al.*, 2002; *Guasta*, 2002; *Mårtensson et al.*, 2006; *Pandithurai et al.*, 2007; *Smirnov et al.*, 2002]. Diurnal variation patterns of AOD, where it is substantially higher during the early morning and late evening hours compared to midday [*Pandithurai et al.*, 2007], would lead to a reduction in cooling during daytime and enhancement in nighttime warming. Enhancement in nighttime warming is also expected for scenarios where there is an increase in black carbon concentrations during the early morning hours [*Allen et al.*, 1999] due to increased emissions from traffic and trapping of aerosols. Other urban sites such as Mexico City [*Smirnov et al.*, 2002] exhibit patterns where the AOD increases during the afternoon hours, thereby enhancing the cooling effect of aerosols. The U3 simulation, in which the daytime AOD is reduced by a factor of one half, was used to examine the impact of the diurnal variation of AOD on surface air temperature. Note that the U3 crudely mimics the AOD diurnal variation reported by *Pandithurai et al.* [2007], where the AOD during the early morning or late afternoon hours is greater than the midday values by a factor of two. Compared to the U1 simulation, the U3 simulation shows an increase in nocturnal surface air temperature (Figure 6) with the nocturnal minimum temperature during the second night being higher by ~0.18°C (Figure 3). However, the DTR in U3 simulation is higher by ~0.79°C due to increase in incoming shortwave compared to the U1 simulation (Figure 3).

[33] Relative humidity enhancement in NBL also creates diurnal asymmetries in AOD, as hygroscopic aerosols respond to a nighttime increase of RH and swell (Figure 5). The impact of hygroscopic swelling in NBL is often insubstantial as the RH increase is confined to a very shallow layer (<100 m), with the maximum swelling of the aerosols occurring at the lowest model level (Figure 5). However, in situations where there are substantial emissions of aerosols into the NBL, significant day-night differences in vertical distribution of aerosols exist [*Guasta*, 2002] and the hygroscopic effect could be important depending upon aerosol composition.

[34] The magnitude of δ_{NBL} and thus response of DTR and mean surface air temperature to aerosol radiative forcing is

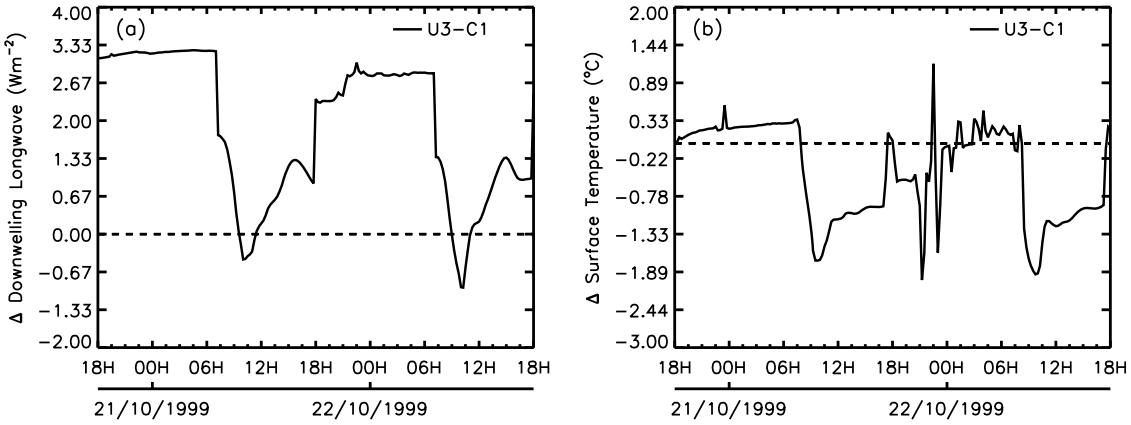

Figure 6. Differences in (a) downwelling longwave fluxes at the surface and (b) surface air temperatures between U3 and C1 experiments. Zero difference value is indicated in Figures 6a and 6b using the dashed line.

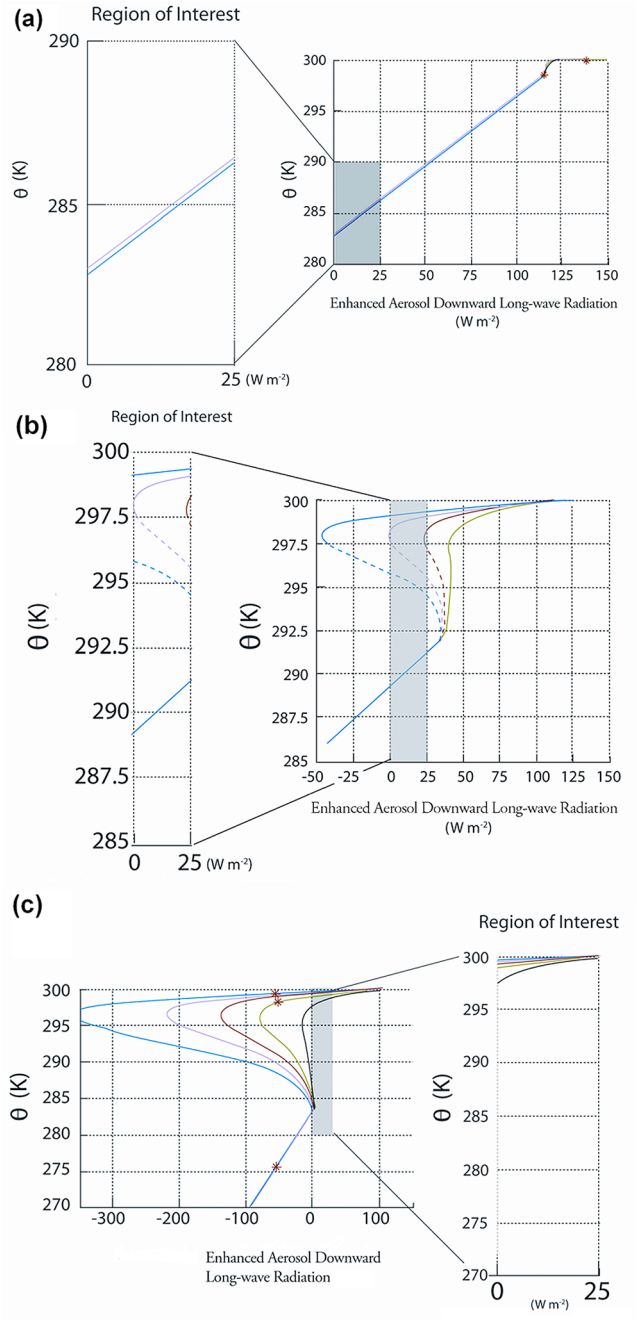

Figure 7. Bifurcation diagrams with enhanced downward radiation from aerosols as the bifurcation parameter (x axis) and boundary layer potential temperature as the response variable (y axis) plotted along the x axis and the boundary layer potential temperature. Line colors give roughness length: green, z_0 = 0.1 m; red, z_0 = 0.25 m; pink, z_0 = 0.5 m; blue, z_0 = 1.0 m. (a) Bifurcation diagram for a geostrophic wind speed of 3 m s^{-1}. (b) Bifurcation diagram for a geostrophic wind speed of 7 m s^{-1}. (c) Bifurcation diagram for a geostrophic wind speed of 10 m s^{-1}.

strongly dependent on NBL dynamics [*Dai and Trenberth*, 2004; *Pielke and Matsui*, 2005; *Walters et al.*, 2007]. A recent study by *Walters et al.* [2007] used nonlinear analysis techniques to examine the sensitivity of the stable nocturnal boundary layer (SNBL) to perturbations in incoming longwave radiation and surface characteristics. *Walters et al.* [2007] found perturbations that decrease NBL stability lead to significant increases in surface temperature. Increase in turbulence that accompany the decrease in NBL stability lead to mixing of warm air from aloft causing rapid, significant changes in surface air temperature. Average longwave nocturnal radiative forcing of 3.0 W m^{-2} found in the U1 simulations is within the range of perturbations reported by *Walters et al.* [2007] to be capable of substantially altering the surface air temperature in the NBL through destabilization. However, the present study may not fully capture the destabilization of the NBL as noted by *Walters et al.* [2007] since the destabilization only occurs when the NBL is near a threshold of transitioning between a strongly stable NBL and weakly stable NBL. Figure 7, created using the bifurcation diagram techniques reported by *Walters et al.* [2007], illustrates this potential transition. Under light winds (Figure 7a), the additional downward radiation produces an increasing temperature in the NBL with a slope (or sensitivity as discussed above) of about 12 K/W m^{-2}. Under strong winds, when the NBL depth is greater, the simple model indicates less sensitivity. However, with intermediate winds, the temperature difference between the two states can be of the order 7–9 K and a sensitivity of 0.28–0.36 K/W m^{-2}. On the basis of the shape of the temperature time series, the first CASES night is probably within the strongly stable case and the second night not quite as stable. However, it may be that the roughness and wind speed are not at the transition parameter space discussed by *Walters et al.* [2007], which can lead to amplified sensitivity. Thus, it may be that other nights may be at this transitional threshold. Only a few nights each year, when the aerosols cause the transition to a warmer boundary layer, are needed to produce a larger climatological temperature difference than that reported in this study.

[35] Soil moisture impacts the partitioning of net radiation received at the surface and thus plays an important role in the diurnal evolution of surface air temperature. Since the soil moisture determines the amount of water vapor added to the boundary layer during the day, it also modulates the aerosol longwave radiative forcing. In order to examine the impact of soil moisture on aerosol nocturnal longwave radiative forcing, the C1 and U1 simulations were repeated with soil saturation increased uniformly throughout the depth of the soil layer to 70%, referred hereon as C2 and U4 simulations. Differences in downwelling longwave radiation between C2 and U4 (Figure 8a) during the second night are substantially smaller compared to the differences found in the C1 and U1 simulations (Figure 2b). The decrease in nocturnal radiative forcing occurs in the higher soil moisture situation, because the C2 simulation develops a substantially moister boundary layer compared to the U4 simulation during the first day. Enhancement of water vapor in the C2 simulation leads to an increase in downwelling longwave radiation partially offsetting the increase in downwelling longwave radiation in U4 from aerosol loading resulting in a smaller nocturnal SLWRF. Interestingly, comparison of surface air temperature between the C2 and U4 simulations show slight nocturnal warming in the C2 simulation during parts of the second night (Figure 8b). The reason for this behavior is not understood and illustrates the complex nonlinear interactions exhibited by the NBL dynamics.

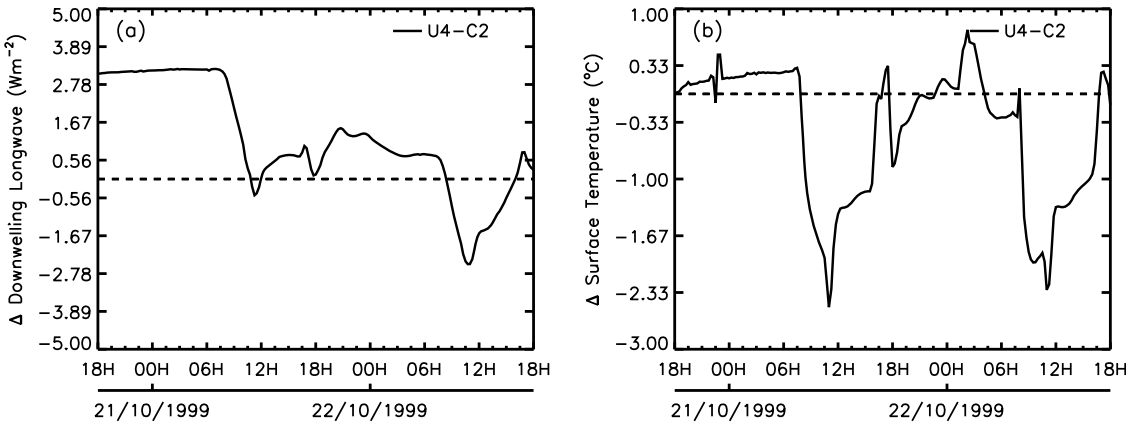

Figure 8. Differences in (a) downwelling longwave fluxes at the surface and (b) surface air temperatures between the U4 and C2 experiments. Zero difference value is indicated in Figures 8a and 8b using the dashed line.

[36] Of all the experiments considered, C2 and U4 show the most dramatic change in DTR when compared to C1 (Figure 3). The difference in DTR between C2, U4, and C1 are −7.3°C and −8.4°C, while the DTR differences between other experiments and C1 are in the range −0.2°C to −2°C. When compared to C1, even though the daytime maximum temperature in the C2 and U4 experiments are reduced by more than −5.9°C, the nocturnal minimum temperature is higher in C2 and U4 by more than 1.2°C. The reason for this strong nocturnal warming, despite strong surface air cooling during the daytime (Table 4), is due to a combination of factors including increased soil heat capacity and bare soil emissivity and an increase in boundary layer moisture during the second day. The impact of enhanced boundary layer moisture in the C2 and U4 experiments is obvious during the second night when the maximum differences in downwelling longwave radiation between both these experiments and C1 exceed 6 W m^{-2}. *Christy et al.* [2006] found an increasing trend in the nocturnal minimum temperature in irrigated regions of central California and suggested changes in soil heat capacity and enhanced water vapor concentration in the boundary layer as possible reasons. The C2 and U4 experiments in this study do indeed support this hypothesis.

[37] The validity of results obtained from the sensitivity analysis for CASES-99 days is further tested in paired numerical experiments C3, U5 and C4, U6, where urban land surface characteristics and aerosol optical characteristics deduced from observations over Pune and Delhi are imposed (Tables 1 and 2). The paired experiments C3, U5 and C4, U6 are conducted for a set of six case study days selected for each of the Pune (3, 4, 8, 17, and 20 January and 2 February 2005) and Delhi sites (6, 8, 7, and 23 April and 1 and 30 May 2003). Note that these case days are relatively clear days, selected to coincide with period for which aerosol optical characteristics were made by *Panicker et al.* [2008] and *Singh et al.* [2005]. While the diurnal variation of downwelling longwave radiation and 2 m surface temperature for the Pune site (Figures 9a and 9b) in the C3 experiment is not substantially higher than found in the C1 experiment, the diurnal variation at the Delhi site shows substantially higher temperatures and downwelling longwave radiation at the surface (Figures 9e and 9f). For the Pune site, the U5 experiments show statistically significant nocturnal SLWRF (Figure 9c) during both the first and second night, with a nocturnal average mean difference of 3.91 and 4.93 W m^{-2} found during the first and second night, respectively. Comparison of the U6 and C4 experiments for the Delhi site also shows statistically significant nocturnal SLWRF (Figure 9d), but the magnitudes are substantially higher compared with the Pune site. Nocturnal average mean differences during the first and second night at the Delhi site are both ~47.7 W m^{-2}, which is substantially higher than that found in all the other experiments. Note that the higher values of nocturnal SLWRF for the Delhi site is partly due to substantially higher surface temperatures compared to other experiments. The mean differences in 2 m temperature between the U5 and C3 experiments are positive and statistically significant through approximately all hours of the first night (Figure 9d). Despite substantial daytime cooling during the first day in the U3 experiments, statistically significant, positive mean differences in 2 m temperature is found in the U3 experiments after ~2300 LST during the second night (Figure 9d). Nocturnal average mean differences in 2 m temperatures for the Pune site are 0.34°C and 0.29°C during the first and second nights, respectively. At the Delhi site, the SLWRF leads to a consistent, statistically significant, positive mean difference in surface 2 m temperatures between the U6 and C4 experiments during both first and second night (Figure 9h). Nocturnal average mean differences in 2 m temperatures for the Delhi site are substantially higher compared to Pune, with values of 2.94°C and 3.13°C found during the first and second nights, respectively. Note that the magnitude of difference between the control experiment and the observations is larger compared to differences between control and other experiments. However, larger differences between the control experiment and the observations are expected since the 1-D modeling framework does not account for the effects of horizontal heterogeneity including large-scale advection.

[38] The paired experiments conducted in this study (U1 and C1, U5 and C3, U6 and C4) show that there is con-

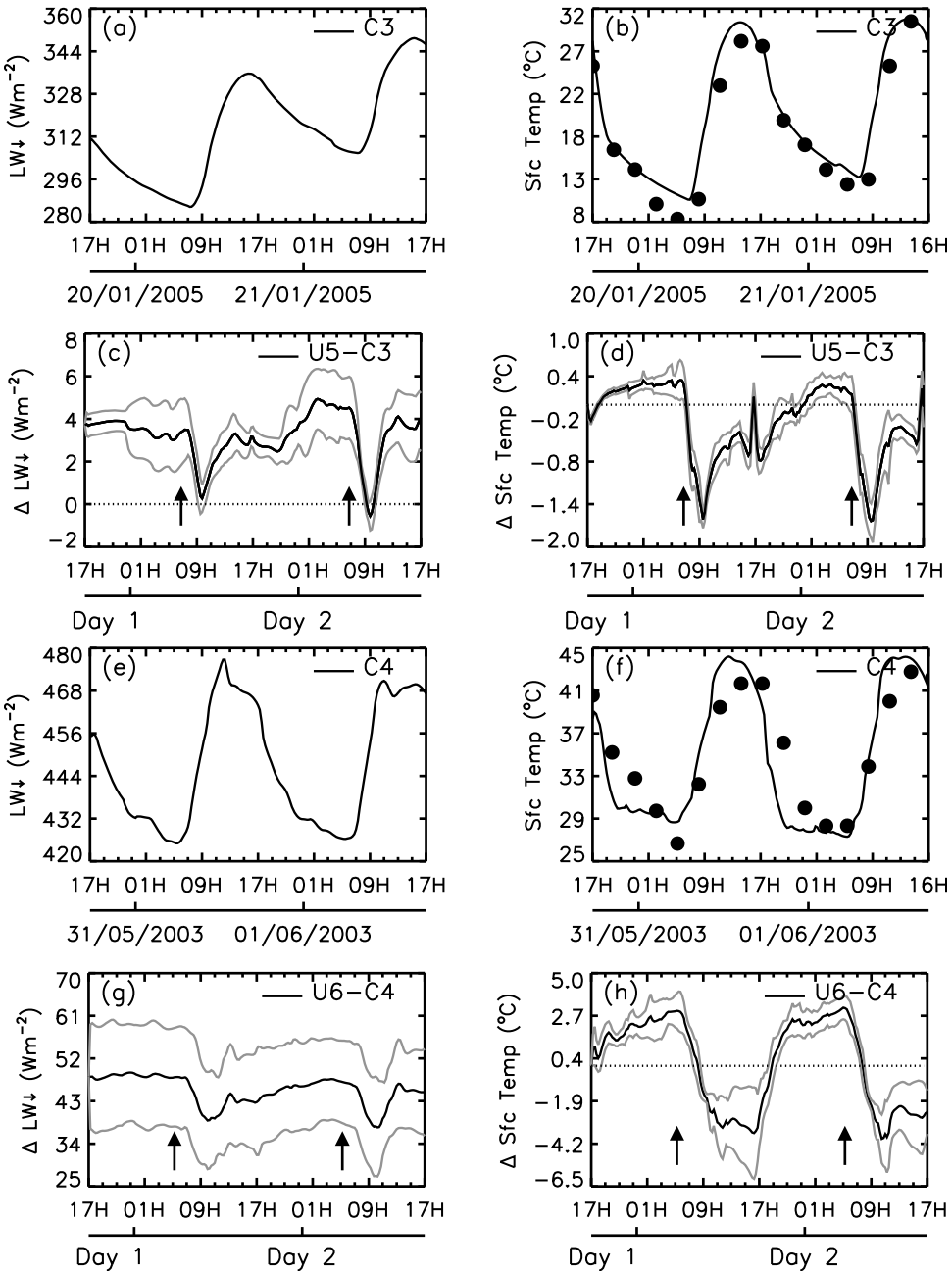

Figure 9. (a) Typical diurnal variation of downwelling longwave radiation at the surface and 2 m temperature for one of the six 48 h periods utilized in the C3 experiment (19–21, 2005). (b) The three hourly observations of 2 m temperature are shown using back dots. (c and d) The diurnal variation of mean difference in downwelling longwave and 2 m temperature between the U5 and C3 experiments for all 6 days used in the study, respectively. The mean difference is shown using a solid black line, while the 95% confidence envelope is shown using the gray lines. Zero difference values in these panels are shown using a dashed black line. (e–h) Same as Figures 9a–9d, except that Figures 9e and 9f pertain to the C4 experiment conducted for 30 May to 1 June 2005 and Figures 9g and 9h show the differences for the U6 and C4 experiments.

siderable variability in the magnitude of nocturnal SLWRF resulting from urban aerosols and its impact on nocturnal minimum temperature. Minimum impact of the enhancement in SLWRF is to compensate for the daytime cooling (Figure 2c), while maximum impact is to a cause a significant nighttime warming (Figures 9d and 9h).

[39] The numerical modeling experiments exhibit differing responses of SLWRF and nocturnal warming to variations in aerosol microphysics and composition. The composition and microphysics of aerosols in the U1 experiment are such that it substantially impacts both the downwelling shortwave and longwave radiation. Water soluble aerosol components

(nitrates and sulfates) in the U1 experiment, with smaller particle size and large number concentrations, lead to a substantial reduction in daytime downwelling shortwave due to scattering. The soot aerosol component (black carbon) in the U1 experiment contributes to absorption in both the shortwave and longwave part of the spectrum. In contrast, the coarse mode mineral component with larger particle sizes in the D1 and U6 experiments are substantially more effective absorbers of longwave radiation and leads to higher values of SLWRF that overwhelm the cooling caused by the daytime reduction in downwelling shortwave radiation.

[40] The numerical experiments considered in this study show a complex response of diurnal surface air temperature variation to urban atmospheric aerosol loading (Figure 3). It is essential to consider aerosol impacts when interpreting surface temperature records in areas such as China, India, and Africa. However, accounting for the aerosol contribution is difficult since the surface air temperature response is dependent on spatial and temporal variations in aerosol concentration, optical characteristics, and is also modulated by other factors such as soil moisture, land surface characteristics, etc.

5. Conclusions

[41] Aerosol radiative forcing plays an important role in boundary layer development and surface temperature evolution. In the context of global climate change, there is considerable interest in the role of aerosols on the climate system especially surface temperature. Previous focus of the research effort in this area has been on shortwave radiative forcing with little attention paid to the impact of longwave radiative forcing, which may be amplified through nocturnal boundary layer dynamics. Since there is a disproportionate nocturnal contribution to warming trends detected in surface temperature records [*Karl et al.*, 1993], it is important to understand the impact of aerosol radiative forcing on nocturnal boundary layer development. This study uses two typical cases of SNBL from the CASES-99 field experiment to examine the impact of urban aerosol radiative forcing on SNBL. For the case study days considered in this study, it is found that:

[42] 1. Urban aerosols have a statistically significant nocturnal downwelling longwave radiative forcing impact at the surface similar to or far exceeding that from doubled atmospheric carbon dioxide at local scales, depending on aerosol composition. Enhanced nocturnal downwelling longwave from urban aerosols compensate for the daytime cooling due to a reduction in downwelling solar radiation. When diurnal variations in AOD are minimal and aerosol absorption in the longwave is modest, urban aerosols maintain the nocturnal minimum surface air temperature the same as that found for clear atmosphere even though the daytime maximum is higher for clear-sky conditions. However, aerosol composition that substantially absorb in the longwave part of the spectrum leads to significant nocturnal warming.

[43] 2. Sensitivity of surface air temperature to radiative forcing is higher by a factor of more than 3 in the NBL compared to CBL since the energy changes impact a shallower layer during the nighttime.

[44] 3. Aerosol radiative characteristics and diurnal asymmetries in AOD play an important role in determining the overall impact of aerosols on surface air temperature.

[45] 4. An increase in downwelling longwave radiation at the surface caused by urban aerosols is of sufficient magnitude to cause destabilization of the marginally stable NBL and significant surface air temperature fluctuations from enhanced vertical mixing as suggested by *Walters et al.* [2007].

[46] 5. The impact of urban aerosol longwave radiative forcing is strongly modulated by soil moisture. SLWRF due to urban aerosols decreases for conditions of higher soil moisture. This is because with higher soil moisture conditions, the boundary layer water vapor content is enhanced under clear-sky conditions, leading to an increase in downwelling longwave at the surface.

[47] In order to understand the impact of urban aerosols on surface air temperature and DTR, detailed knowledge regarding diurnal variation of aerosol characteristics including vertical distribution, optical properties, and column loading are needed. Further modeling studies are necessary to examine the impact of aerosol radiative forcing on the marginally stable NBL. Once the NBL conditions most sensitive to urban aerosol radiative forcing are identified, the frequency of occurrence of such conditions need to be determined from observations. Such analysis will allow quantification of the aerosol radiative forcing contribution to observed nocturnal warming trends. The 1-D numerical modeling framework utilized in this study results in the differences between the observations and control experiments being larger than the differences between the sensitivity experiments. Three-dimensional numerical model experiments that account for atmospheric horizontal heterogeneity are also required for future studies.

[48] **Acknowledgments.** This research was supported by DOE grant DE-FG02-05ER45187 and NSF grant ATM-0417774. Sundar Christopher was supported by NASA Radiation Sciences Program. We would also like to thank Jonathan G. Fairman Jr. for assistance with the preparation of the figures.

References

Allen, G. A., J. Lawrence, and P. Koutrakis (1999), Field validation of a semicontinuous method for aerosol black carbon (aethalometer) and temporal patterns of summertime hourly black carbon measurements in southwestern PA, *Atmos. Environ.*, *33*, 817–823, doi:10.1016/S1352-2310(98)00142-3.

Balling, R. C., Jr., and R. S. Cerveny (2003), Vertical dimensions of seasonal trends in the diurnal temperature range across the central United States, *Geophys. Res. Lett.*, *30*(17), 1878, doi:10.1029/2003GL017776.

Braganza, K., D. J. Karoly, and J. M. Arblaster (2004a), Diurnal temperature range as an index of global climate change during the 20th century, *Geophys. Res. Lett.*, *31*, L13217, doi:10.1029/2004GL019998.

Braganza, K., D. J. Karoly, A. C. Hirst, A. C. Hirst, P. Stott, R. J. Stouffer, and S. F. B. Tett (2004b), Simple indices of global climate variability and change: Part II. Attribution of climate change during the 20th century, *Clim. Dyn.*, *22*, 823–838, doi:10.1007/s00382-004-0413-1.

Cao, H. X., J. F. B. Mitchell, and J. R. Lavery (1992), Simulated diurnal range and variability of surface temperature in a global climate model for present and doubled CO_2 climates, *J. Clim.*, *5*, 920–943, doi:10.1175/1520-0442(1992)005<0920:SDRAVO>2.0.CO;2.

Chen, C., and W. R. Cotton (1983), A one-dimensional simulation of the stratocumulus-capped mixed layer, *Boundary Layer Meteorol.*, *25*, 289–321, doi:10.1007/BF00119541.

Chen, F., et al. (2007), Description of evaluation of the characteristics of the NCAR high-resolution land data assimilation system during IHOP-02, *J. Appl. Meteorol.*, *46*, 694–713, doi:10.1175/JAM2463.1.

Christopher, S. A., J. Wang, Q. Ji, and S.-C. Tsay (2003), Estimation of shortwave dust aerosol radiative forcing during PRIDE, *J. Geophys. Res.*, *108*(D19), 8596, doi:10.1029/2002JD002787.

Christy, J. R., W. B. Norris, K. Redmond, and K. P. Gallo (2006), Methodology and results of calculating central California surface temperature trends: Evidence of human-induced climate change?, *J. Clim.*, *19*, 548–563, doi:10.1175/JCLI3627.1.

Cotton, W. R., R. A. Pielke, R. L. Walko, G. E. Liston, and C. J. Tremback (2003), RAMS 2001: Current status and future directions, *Meteorol. Atmos. Phys.*, *82*, 5–29, doi:10.1007/s00703-001-0584-9.

Dai, A., and K. E. Trenberth (2004), The diurnal cycle of its depiction in the Community Climate System Model, *J. Clim.*, *17*, 930–951, doi:10.1175/1520-0442(2004)017<0930:TDCAID>2.0.CO;2.

Dai, A., K. E. Trenberth, and T. R. Karl (1999), Effects of clouds, soil moisture, precipitation, and water vapor temperature range, *Int. J. Climatol.*, *12*, 2451–2473, doi:10.1175/1520-0442(1999)012<2451:EOCSMP>2.0.CO;2.

Dorsey, J. R., E. Nemitz, M. W. Gallagher, D. Fowler, P. I. Williams, K. N. Bower, and K. M. Beswick (2002), Direct measurements and parameterisation of aerosol flux, concentration and emission velocity above a city, *Atmos. Environ.*, *36*, 791–800, doi:10.1016/S1352-2310(01)00526-X.

Estournel, C., R. Vehil, D. Guedalia, J. Fontan, and A. Druilhet (1983), Observations and modeling of downward radiative fluxes (solar and infrared) in urban/rural areas, *J. Clim. Appl. Meteorol.*, *22*, 134–142, doi:10.1175/1520-0450(1983)022<0134:OAMODR>2.0.CO;2.

Fu, Q., and K. N. Liou (1992), On the correlated k-distribution method for radiative transfer in nonhomogeneous atmospheres, *J. Atmos. Sci.*, *49*, 2139–2156, doi:10.1175/1520-0469(1992)049<2139:OTCDMF>2.0.CO;2.

Fu, Q., and K. N. Liou (1993), Parameterization of the radiative properties of cirrus clouds, *J. Atmos. Sci.*, *50*, 2008–2025, doi:10.1175/1520-0469(1993)050<2008:POTRPO>2.0.CO;2.

Garratt, J. R., A. B. Pittock, and K. Walsh (1990), Response of the atmospheric boundary layer and soil layer to a high altitude, dense aerosol cover, *J. Appl. Meteorol.*, *29*, 35–52, doi:10.1175/1520-0450(1990)029<0035:ROTABL>2.0.CO;2.

Guasta, M. D. (2002), Daily cycles in urban aerosols observed in Florence (Italy) by means of an automatic 532–1064 nm LIDAR, *Atmos. Environ.*, *36*, 2853–2865, doi:10.1016/S1352-2310(02)00136-X.

Hansen, J., M. Sato, and R. Ruedy (1995), Long-term changes of the diurnal temperature cycle: Implications about mechanisms of global climate change, *Atmos. Res.*, *37*, 175–209, doi:10.1016/0169-8095(94)00077-Q.

Harrington, J. Y., T. Reisin, W. R. Cotton, and S. M. Kreidenweis (1999), Cloud resolving simulations of Arctic stratus: Part II. Transition-season clouds, *Atmos. Res.*, *51*, 45–75, doi:10.1016/S0169-8095(98)00098-2.

Hess, M., P. Koepke, and I. Schult (1998), Optical properties of aerosols and clouds: The software package OPAC, *Bull. Am. Meteorol. Soc.*, *79*, 831–844, doi:10.1175/1520-0477(1998)079<0831:OPOAAC>2.0.CO;2.

Intergovernmental Panel on Climate Change (IPCC) (2007), *Climate Change 2007: The Physical Science Basis. Contribution of Working Group I to the Fourth Assessment Report of the Intergovernmental Panel on Climate change*, edited by S. Solomon et al., Cambridge Univ. Press, Cambridge, U. K.

Jacobson, M. Z. (1997), Development and application of a new air pollution modeling system: Part III. Aerosol-phase simulations, *Atmos. Environ.*, *31*, 587–608, doi:10.1016/S1352-2310(96)00201-4.

Kalnay, E., and M. Cai (2003), Impact of urbanization and land-use change on climate, *Nature*, *423*, 528–531, doi:10.1038/nature01675.

Karl, T. R., G. Kukla, and J. Gavin (1984), Decreasing diurnal temperature range in the United States and Canada from 1941 through 1980, *Int. J. Climatol.*, *23*, 1489–1503, doi:10.1175/1520-0450(1984)023.

Karl, T. R., P. D. Jones, R. W. Knight, G. Kukla, N. Plummer, V. Razuvayev, K. P. Gallo, J. Lindseay, R. J. Charlson, and T. C. Peterson (1993), A new perspective on recent global warming: Asymmetric trends of daily maximum and minimum temperature, *Bull. Am. Meteorol. Soc.*, *74*, 1007–1023, doi:10.1175/1520-0477(1993)074<1007:ANPORG>2.0.CO;2.

Koch, D., T. C. Bond, D. Streets, N. Unger, and G. R. V. D. Werf (2007), Global impacts of aerosols from particular source regions and sectors, *J. Geophys. Res.*, *112*, D02205, doi:10.1029/2005JD007024.

Mahrer, Y., and R. A. Pielke (1977), The effects of topography on sea and land breezes in a two-dimensional numerical model, *Mon. Weather Rev.*, *105*, 1151–1162, doi:10.1175/1520-0493(1977)105<1151:TEOTOS>2.0.CO;2.

Makowski, K., M. Wild, and A. Ohmura (2008), Diurnal temperature range over Europe between 1950 and 2005, *Atmos. Chem. Phys. Discuss.*, *8*, 7051–7084, doi:10.5194/acpd-8-7051-2008.

Mårtensson, E. M., E. D. Nilsson, G. Buzorius, and C. Johansson (2006), Eddy covariance measurements and parameterisation of traffic related particle emissions in an urban environment, *Atmos. Chem. Phys.*, *6*, 769–785, doi:10.5194/acp-6-769-2006.

Pandithurai, G., R. T. Pinker, P. C. S. Devara, T. Takamura, and K. K. Dani (2007), Seasonal asymmetry in diurnal variation of aerosol optical characteristics over Pune, western India, *J. Geophys. Res.*, *112*, D08208, doi:10.1029/2006JD007803.

Panicker, A. S., G. Pandithurai, P. D. Safai, and S. Kewat (2008), Observations of enhanced aerosol longwave radiative forcing over an urban environment, *Geophys. Res. Lett.*, *35*, L04817, doi:10.1029/2007GL032879.

Pielke, R. A., and T. Matsui (2005), Should light wind and windy nights have the same temperature trends at individual levels even if the boundary layer averaged heat content change is the same?, *Geophys. Res. Lett.*, *32*, L21813, doi:10.1029/2005GL024407.

Pielke, R. A., Sr., et al. (2007), Unresolved issues with the assessment of multidecadal global land temperature trends, *J. Geophys. Res.*, *112*, D24S08, doi:10.1029/2006JD008229.

Poulos, G. S., et al. (2002), CASES-99: A comprehensive investigation of the stable nocturnal boundary layer, *Bull. Am. Meteorol. Soc.*, *83*, 555–581, doi:10.1175/1520-0477(2002)083<0555:CACIOT>2.3.CO;2.

Ramanathan, V., P. J. Crutzen, J. T. Kiehl, and D. Rosenfeld (2001a), Aerosols, climate, and the hydrological cycle, *Science*, *294*, 2119–2124, doi:10.1126/science.1064034.

Ramanathan, V., et al. (2001b), Indian Ocean Experiment: An integrated analysis of the climate forcing and effects of the great Indo-Asian haze, *J. Geophys. Res.*, *106*(D22), 28,371–28,398, doi:10.1029/2001JD900133.

Singh, S., S. Nath, R. Kohli, and R. Singh (2005), Aerosols over Delhi during premonsoon months: Characteristics and effects on surface radiation forcing, *Geophys. Res. Lett.*, *32*, L13808, doi:10.1029/2005GL023062.

Smirnov, A., B. N. Holben, T. F. Eck, I. Slutsker, B. Chatenet, and R. T. Pinker (2002), Diurnal variability of aerosol optical depth observed at AERONET (Aerosol Robotic Network) sites, *Geophys. Res. Lett.*, *29*(23), 2115, doi:10.1029/2002GL016305.

Steeneveld, G. J., B. Wiel, and A. A. M. Holstag (2006), Modeling the evolution of the atmospheric boundary layer coupled to the land surface for three contrasting nights in CASES-99, *J. Atmos. Sci.*, *63*, 920–935, doi:10.1175/JAS3654.1.

Stone, D. A., and A. J. Weaver (2003), Factors contributing to diurnal temperature range trends in twentieth and twenty-first century simulations of the CCCma coupled model, *Clim. Dyn.*, *20*, 435–445.

Venkatram, A., and R. Viskanta (1977), Radiative effects of elevated pollutant layers, *J. Appl. Meteorol.*, *16*, 1256–1272, doi:10.1175/1520-0450(1977)016<1256:REOEPL>2.0.CO;2.

Vose, R. S., D. R. Easterling, and B. Gleason (2005), Maximum and minimum temperature trends for the globe: An update through 2004, *Geophys. Res. Lett.*, *32*, L23822, doi:10.1029/2005GL024379.

Walko, R. L., et al. (2000), Coupled atmosphere-biophysics-hydrology models for environmental modeling, *J. Appl. Meteorol.*, *39*, 931–944, doi:10.1175/1520-0450(2000)039<0931:CABHMF>2.0.CO;2.

Walters, J. T., R. T. McNider, X. Shi, W. B. Norris, and J. R. Christy (2007), Positive surface temperature feedback in the stable nocturnal boundary layer, *Geophys. Res. Lett.*, *34*, L12709, doi:10.1029/2007GL029505.

Wang, J., and S. A. Christopher (2006), Mesoscale modeling of Central American smoke transport to the United States: 2. Smoke radiative impact on regional surface energy budget and boundary layer evolution, *J. Geophys. Res.*, *111*, D14S92, doi:10.1029/2005JD006720.

Wang, J., S. A. Christopher, U. S. Nair, J. S. Reid, E. M. Prins, J. Szaykman, and J. L. Hand (2006), Mesoscale modeling of Central American smoke transport to the United States: 1. "Top-down" assessment of emission strength and diurnal variation impacts, *J. Geophys. Res.*, *111*, D05S17, doi:10.1029/2005JD006416.

Welch, R., and W. Zdunkowski (1976), A radiation model of the polluted atmospheric boundary layer, *J. Atmos. Sci.*, *33*, 2170–2184, doi:10.1175/1520-0469(1976)033<2170:ARMOTP>2.0.CO;2.

Yu, H., S. C. Liu, and R. E. Dickinson (2002), Radiative effects of aerosols on the evolution of the atmospheric boundary layer, *J. Geophys. Res.*, *107*(D12), 4142, doi:10.1029/2001JD000754.

Zdunkowski, W. G., R. M. Welch, and J. Paegle (1976), One-dimensional numerical simulation of the effects of air pollution on the planetary boundary layer, *J. Atmos. Sci.*, *33*, 2399–2414, doi:10.1175/1520-0469(1976)033<2399:ODNSOT>2.0.CO;2.

Zhou, L., R. E. Dickinson, Y. Tian, R. S. Vose, and Y. Dai (2007), Impact of vegetation removal and soil aridation on diurnal temperature range in a semiarid region: Application to the Sahel, *Proc. Natl. Acad. Sci. U. S. A.*, *104*, 17,937–17,942, doi:10.1073/pnas.0700290104.

Zobler, L. (1999), Global Soil Types, 1-Degree Grid (Zobler), http://www.daac.ornl.gov, Oak Ridge Natl. Lab., Oak Ridge, Tenn.

S. A. Christopher, K. Fuller, and U. S. Nair, Earth System Science Center, University of Alabama in Huntsville, 320 Sparkman Dr., Huntsville, AL 35805, USA. (nair@nsstc.uah.edu)

R. McNider, Department of Atmospheric Science, University of Alabama in Huntsville, 320 Sparkman Dr., Huntsville, AL 35805, USA.

F. Patadia, Goddard Earth Sciences and Technology Center, University of Maryland, Baltimore County, Baltimore, MD 21228, USA.